NANO LETTERS

2009
Vol. 9, No. 5
1866-1871

Charge Transport in Interpenetrating Networks of Semiconducting and Metallic Carbon Nanotubes

Mark A. Topinka,[†,‡,||] Michael W. Rowell,[†,||] David Goldhaber-Gordon,[*,‡,||] Michael D. McGehee,[†,||] David S. Hecht,[§] and George Gruner[§]

Materials Science and Engineering Department, Physics Department, Stanford University, Stanford, California, Physics Department, University of California Los Angeles, Los Angeles, California, and Stanford Institute for Materials and Energy Sciences, SLAC National Accelerator Laboratory, Menlo Park, California

Received December 19, 2008; Revised Manuscript Received February 25, 2009

Downloaded by STANFORD UNIV GREEN LIBR on June 30, 2009
Published on May 13, 2009 on http://pubs.acs.org | doi: 10.1021/nl803849e

ABSTRACT

Carbon nanotube network field effect transistors (CNTN-FETs) are promising candidates for low cost macroelectronics. We investigate the microscopic transport in these devices using electric force microscopy and simulations. We find that in many CNTN-FETs the voltage drops abruptly at a point in the channel where the current is constricted to just one tube. We also model the effect of varying the semiconducting/metallic tube ratio. The effect of Schottky barriers on both conductance within semiconducting tubes and conductance between semiconducting and metallic tubes results in three possible types of CNTN-FETs with fundamentally different gating mechanisms. We describe this with an electronic phase diagram.

Carbon nanotubes are increasingly being used in the form of random network films for electronic applications. Thin (submonolayer) CNT films have been demonstrated as a material for low cost flexible transparent field effect transistors (FETs),[1−7] as well as for gas, pH, chemical, DNA, and optical/IR sensors.[8−11] The best CNTN-FETs to date have reached high ON/OFF ratios around 10^5 while at the same time achieving field effect mobilities on the order of 10 cm^2/Vs[1] for as-produced-films and 80 cm^2/Vs[12] for films where additional processing has been used to break metallic network conduction. Individual nanotubes have been shown to have mobilities as high as 10 000 cm^2/Vs[13] to 100 000 cm^2/Vs[14]. The reasons for the large gap between film mobilities and individual tube mobilities is still not fully understood, and there could potentially be significant room for improvement in device performance by controlling the density, tube-tube junction characteristics, and semiconducting fraction of tubes.

A factor that makes CNT films complex is that they contain both metallic and semiconducting tubes. Since the semiconducting tubes are frequently doped, both kinds of tubes can carry current.[14,15] Only the semiconducting tubes can have their conductance significantly modulated by the gate in an FET. The switching mechanism in CNTN-FETs can be due to modulation of the Schottky barriers between semiconducting tubes and metallic tubes[16−18] or metal contacts.[19] It could also be due to modulation of semiconducting tube conductance either by controlling the carrier density or by modulating Schottky barriers in semiconducting tubes formed by defects or overlaps with metallic tubes.[1,20] Depending on the fabrication technique and semiconducting/metallic ratio, any or all of these mechanisms may be at play.

Regardless of which switching mechanism is actually responsible for a CNTN-FET's operation, in order to have a high ON/OFF ratio it is critical to have a percolative network of tubes that can be modulated by the gate but not to have a percolative metallic network that would short out the device. There have been a few different proposals for dealing with this problem. One approach recently demonstrated is to lithographically pattern the channel dimensions such that the channel is long and narrow with respect to the tube lengths, which breaks percolation in the metallic network.[12] A second approach is to deposit relatively high-density percolative films, gate the semiconducting tubes "off", and apply a large drain-source voltage pulse to burn out the metallic network, or at least a few critical metallic tubes or junctions.[3,21] Though these approaches work, the additional cost of implementing them could offset the benefits of low-cost solution processing and printing. A third is to very carefully control the tube density and tube length such that

* To whom correspondence should be addressed. E-mail: goldhaber-gordon@stanford.edu.
[†] Materials Science and Engineering Department, Stanford University.
[‡] Physics Department, Stanford University.
[§] University of California Los Angeles.
[||] SLAC National Accelerator Laboratory.

10.1021/nl803849e CCC: $40.75 © 2009 American Chemical Society
Published on Web 03/30/2009

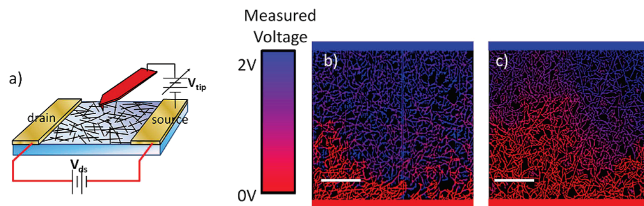

Figure 1. (a) Schematic showing the measurement technique used to image voltage drops in CNT films. A voltage, V_{ds}, is applied across the device with the backgate held at a fixed voltage. A tip is then scanned over the device in surface-potential mapping mode to collect detailed information about where the voltage drops (and hence where the resistance in the film lies) through the device. (b,c) Experimental images on nominally identical devices (40 × 40 μm, same average tube length, density, diameter, and type). Panel b shows a large potential "cliff" near the bottom electrode and exhibits a relatively high resistance of 630 kΩ, while panel c displays a smooth voltage drop between drain and source and a much lower resistance of 65 kΩ.

Downloaded by STANFORD UNIV GREEN LIBR on June 30, 2009
Published on May 13, 2009 on http://pubs.acs.org | doi: 10.1021/nl803849e

there are percolative paths through the semiconducting tubes but not the metallic tubes. This approach would seem possible because there are two semiconducting tubes for every metallic tube in a typical ensemble with uncontrolled chirality. The fourth approach is to sort,[22−25] etch,[26] or grow[27,28] the tubes to achieve a high ratio of semiconducting to metallic tubes.

These different device fabrication techniques will likely lead to devices with different switching behavior and variability from percolation effects. For this, we investigate how current flows through CNTN-FETs near percolation using a combination of standard conductance measurements, quantitative electric force microscopy (EFM) and numerical simulations. We provide a calculated phase diagram that shows which mechanisms determine the behavior of working CNTN-FETs depending on the tube density and ratio of semiconducting to metallic tubes. The numerical simulations and phase diagram show, for example, that CNTN-FETs based on standard 2/3 semiconducting 1/3 metallic CNT mixes will, regardless of tube density, have their semiconducting tubes blocked or modulated by Schottky barriers induced by crossings with metallic tubes.

To begin investigating the sources of resistance in different types of CNTN-FETs, we have employed EFM to create maps of where the voltage drops in the films when a current flows through them[29−35] (see Supporting Information for a description of the EFM technique). Our first images are of CVD grown films contacted by 40 μm wide Ti/Au source and drain electrodes with 40 μm spacing. These dimensions are similar to those that would be used for FETs in large area, low-cost circuits. A metal-coated AFM tip is scanned over the film and the surface potential that results from current flow in the FET is imaged (Figure 1a). Figure 1b,c shows EFM images of two FETs fabricated immediately next to each other on the same CVD grown CNT film. The characteristics of the constituent nanotubes, such as the tube density and average lengths, should be the same. However, we see that both the electrical performance and the images of voltage drop across the FET show drastic differences. Device 1 (Figure 1b) is relatively gateable with an ON/OFF ratio of about 10 over $V_g = \pm 3$ V, but with relatively high resistance varying from about 0.3 to 4 MΩ (630 kΩ at $V_g = 0$). This device shows an interesting and unexpected feature in the voltage map (Figure 1b); rather than dropping smoothly from drain to source, the voltage seems to mostly drop across a voltage cliff close to the bottom of the image. This indicates that the resistance of the device is dominated by large resistances in the network located near the voltage cliff. Device 2 (Figure 1c) is relatively ungateable with the resistance changing by less than 30% and has a much lower resistance centered at 65 kΩ. The electrostatic potential map of this device shows a much smoother change in voltage between source and drain, indicating that no single location of high resistance dominates the behavior of the device.

To better understand the source of these observed large variations in electrical performance as well as the presence or absence of voltage cliffs in the images of flow through the CNTN-FETs, we numerically simulate the electrostatic potential and current flow in CNT films (in Figure 2).[7,37−42] Nanotubes of the desired length are sprinkled down in random positions and orientations until the desired density is reached. The resulting set of tube segments and tube junctions is turned into a resistor network and the overall resistance of the network is solved using MATLAB sparse matrix inversion. The length (L) and density (n) range of tubes was chosen to match the devices investigated experimentally in Figure 1 ($L = 4$ μm, $n = 2$ $\mu m_{CNT}/\mu m^2$ or 0.5 tubes/μm^2). Tube resistance was measured using scanned potentiometry (see Supporting Information) to be $R_{tube} = 13$ kΩ/μm, similar to values found in literature,[14,29,43−46] and tube junction resistance, $R_{junction} = 200$ kΩ/junction, was taken from literature.[20] We begin with a simplifying set of assumptions that, given ambient p-type O_2 doping and for $V_g = 0$ V, all nanotubes in the film have similar electrical properties. The effects of having Schottky barriers at the junctions and overlaps between metallic and semiconducting tubes are described later.

We ran the simulation for 300 different random sets of films, varying the density between 0 and 0.75 tubes/μm^2 for each run. The conductance versus density for all 300 of these runs is plotted in Figure 2e. The average conductance for the ensemble of films fits well to the theoretical formula for percolative conduction through sticks in 2d, $G = G_0 (n - n_{perc})^\alpha$ with $n_{perc} = 1/\pi (4.236/L_{tube})^2 = 0.34$ tubes/μm^2, $\alpha = 1.34$ (an ideal theoretical 2d film would give $\alpha = 1.33$) and $G_0 = 5.3 \times 10^{-6} \mu m^2/\Omega$. G_0 and α were made adjustable in the fit while n_{perc} was calculated from percolation theory using the known tube density and length.[36] The simulations reveal important information that is not contained in the percolation equation. There are substantial statistical fluctuations in the conductivity of the networks. Just above the percolation threshold the standard deviation in the conductivity is large compared to the average value. For example, the films with a density of exactly $n = 0.48$ tubes/μm^2 have conductivities that vary by an order of magnitude. To show why these fluctuations exist, we provide in Figure 2a−d current and electrostatic potential maps for one of the least and one of the most conductive films with this density. The

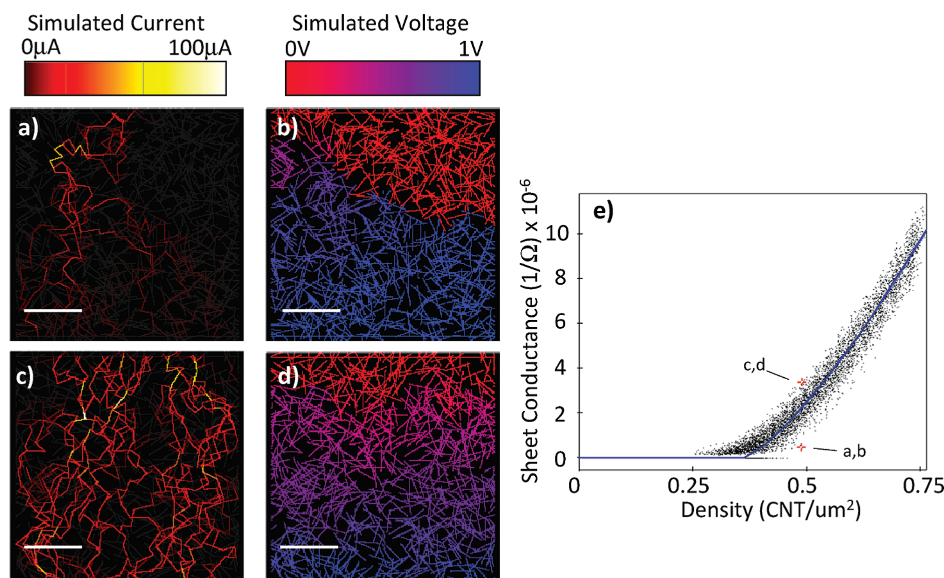

Figure 2. (a−d) Simulated voltage drops (b,d) and current (a,c) across two films with precisely identical tube length and density, with the only difference being the random configuration of the tubes. The corresponding points on plot e are highlighted with red crosses. There is a large difference between the two nominally identical films in terms of voltage drops, current flow, and corresponding resistance even though the films are of exactly the same tube density and length. The parameters for these two simulations were (L = 4 μm, n = 0.5 tubes/μm, size = 40 × 40 μm, R_{tube} = 13 kΩ/μm, R_{junction} = 200 kΩ. (e) shows the conductance as a function of density for 300 different randomly generated series of films. These simulations assume all equally conducting tubes, i.e., all metallic or all heavily doped semiconductor, in order to highlight the unavoidable statistical fluctuations of a device made even with precisely controlled tube length and density. The blue line is a plot of the best fit to percolation theory.[36]

Downloaded by STANFORD UNIV GREEN LIBR on June 30, 2009
Published on May 13, 2009 on http://pubs.acs.org | doi: 10.1021/nl803849e

two films chosen here are outliers, being at roughly 0.5th and 99.5th percentile of conductivity for this density, respectively, but if CNTN-FETs are to be used for small scale integrated circuits incorporating hundreds of FETs, such outliers are important to consider. For the high resistance simulated device (current and voltage shown in Figure 2a,b), the current flows along one or at most a few main paths, and large discrete voltage drops (or cliffs) can occur across the film between areas that are connected by few tubes. With simply a different "roll of the dice", that is, a new device with identical tube density and length but different random tube placement, the electrical characteristics of the film as well as the spatial patterns of flow and voltage drop can change dramatically. For the second simulated film (Figure 2c,d) the current flows along many parallel paths, and the voltage drops smoothly across the device. These simulations suggest a clear explanation for the very different resistances and spatial voltage patterns found in our experimental images in Figures 1b,c. These films are also slightly above the percolation threshold, and hence they have the same large fluctuations in conductivity as well as the presence or absence of voltage cliffs that we see in the simulations. These fluctuations can be expected to be extremely significant for CNTN-FETs produced near the percolation threshold.

Finally, in Figures 3 and 4 we refine the simulations in order to understand the gating in a CNTN-FET when using mixtures of metallic and semiconducting tubes. Previous research has shown that metallic tubes conduct well to other metallic tubes (M−M), and semiconducting tubes conduct well to other semiconducting tubes (S−S), but metallic/semiconducting tube−tube contacts cause a Schottky barrier in the semiconducting tubes that can modulate current flow not only between the metallic and semiconducting tubes (M−S junctions) but also through the affected semiconducting tubes (M−S crossings).[20] Recent simulations of conduction in mixed networks of semiconducting and metallic tubes[39,41,42] have not yet included the effects of the Schottky barrier on conduction through the semiconducting tube itself. Here, in Figure 3, we model the conductance of a CNTN-FET at V_g = 0 V, where M tubes, S tubes (assumed to be ambiently doped), M−M junctions, and S−S junctions are treated as conductive, but at M−S junctions and M−S crossings no current is allowed to flow through the affected semiconducting tubes at points of contact. We do not include any possible effects at the source and drain contacts as we have not observed any potential drops at the Ti/Au electrodes in any of our EFM scans.

Figure 3a−e shows the tube type and current configuration of a series of simulated carbon nanotube networks where tubes, one by one, are switched in the simulation from metallic to semiconducting. The total film density is held at three times the conducting-stick percolation threshold, and the positions of the tubes are not changed, only the type, metallic versus semiconducting, is switched. As would be expected, for all-metallic or all-semiconducting films (Figure 3a,e), because the film is far past the percolation threshold, the current through the film is largely uniform and the conductance is high. As we move away from point A (the all-metallic tube network), the number of metallic tubes is diluted. Beyond 70% semiconducting (Figure 3b and point B in Figure 3e), there is no conduction through the metallic tubes since the metallic tube density is now below the percolation density. What is interesting is that even though at this M/S ratio point the density of semiconducting tubes

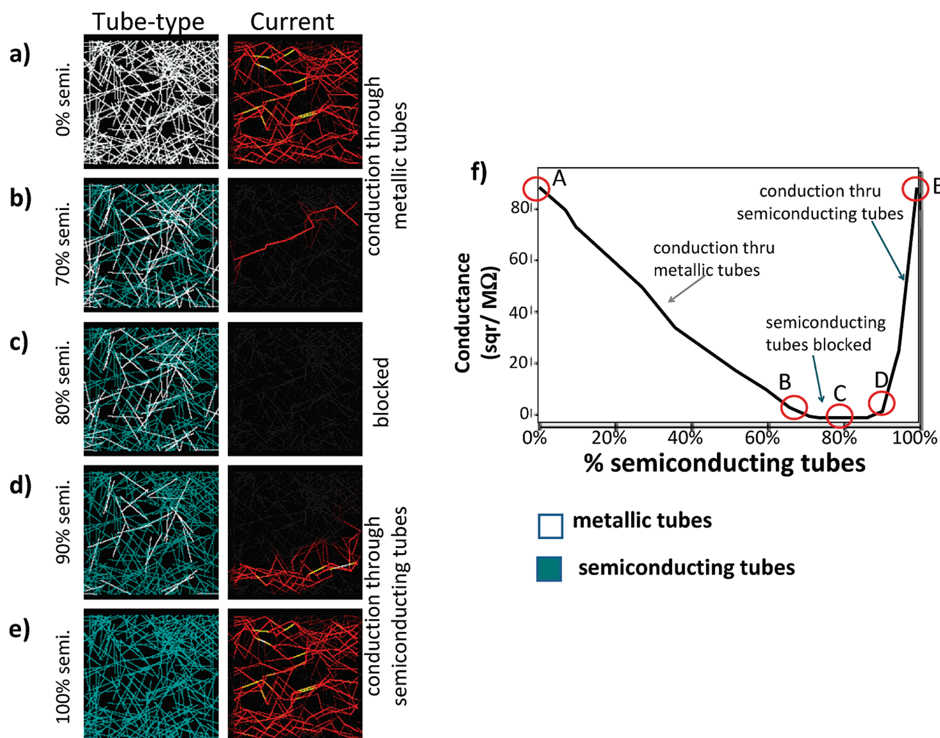

Figure 3. Effect of varying the ratio of metallic (white) and semiconducting (green) tubes where a Schottky barrier forms in the semiconducting tube at M-S crossings and junctions, blocking transport between tubes and through the semiconducting tube.[20] For frames a−e, the tube density, length, locations, and orientations in the films were held constant, but the ratio of semiconducting to metallic tubes was varied. The combination of density and tube length was chosen to be about 3 times the percolation threshold if the tubes were all metallic or all semiconducting. (f) Expected conductance as a function of proportion of semiconducting tubes (assuming for simplicity that an unblocked semiconducting tube conducts as well as a metallic tube, which is a reasonable approximation for ambient O_2 p-doping of semiconducting tubes at V_g=0.[15]).

Downloaded by STANFORD UNIV GREEN LIBR on June 30, 2009
Published on May 13, 2009 on http://pubs.acs.org | doi: 10.1021/nl803849e

is over two times the percolation threshold, modulation of conduction through the semiconducting network can be dominated by Schottky barriers from M-S junctions and crossings within the channel. This situation persists for a range of densities (Figure 3c and point C in Figure 3f) until finally at very low metallic percentage (Figure 3d and point D in Figure 3f), paths through the purely semiconducting network that bypass the M/S crossing points open up, and the modulation of conduction changes to the purley semiconducting network.

Figure 4 is a general phase diagram that describes the nature of a nanotube film as a function of nanotube density and semiconductor fraction. The boundaries between different phases are sharp for very large networks, and for smaller networks represent the statistically most likely type of resulting CNTN-FET given film density and S/M ratio. Because the density of tubes is normalized by the percolation threshold density, this diagram is valid for any length of tube.

For films where the density is too low, the network lies in the dark gray subpercolation regime. The light-gray phase corresponds to densities and S/M ratios where a percolative metallic network will exist, and no significant FET action is likely, at least without the burning out of metallic tubes described previously. Just above percolation in the light green phase labeled "binary network", neither the metallic nor the semiconducting network is above the percolation threshold and so current must pass between the two subnetworks. Conduction will be modulated primarily by M-S junctions and high ON/OFF ratios can be achieved, but the current will generally be quite low since these M-S junctions are highly resistive and the network is sparse. The light and dark blue phases, labeled "blocked" and "unblocked semiconducting network", respectively, are also expected to produce high ON/OFF ratios, but the gating mechanism differs between them. In the light blue "blocked semiconducting networks" regime, the semiconducting tubes are above percolation but are blocked by crossings with metallic tubes. Hence, conduction will be modulated primarily by M−S crossings and high ON/OFF ratios can be achieved. As the semiconducting fraction is increased, we pass from the light blue "blocked" phase into the dark blue "unblocked" phase. In this region of tube density and S/M ratio, at least some pure semiconducting paths between electrodes exist, completely unblocked by any crossings with metallic tubes. Those paths can bypass the highly resistive M-S crossing Schottky barriers.

CNTN-FETs are often assumed to operate in the dark blue "unblocked" phase: an uninterrupted percolative semiconducting network bridges the gap between the electrodes, and gating with a backgate causes the desired large ON/OFF ratios by simply modulating the semiconducting tube conductance. This assumption may not be correct, however. As can be seen from this phase diagram, there is no tube density for the standard S/M ratios of 2/3:1/3 that yields an "unblocked semiconducting network". Consequently, for CNT films made with an unenriched 67% semiconducting fraction, CNTN-FETs must necessarily be in the regime of

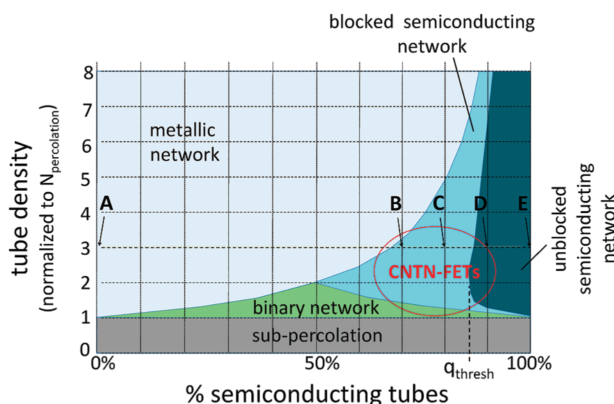

Figure 4. Calculated general phase diagram showing the different possible electronic phases of a mixed metallic-semiconducting carbon nanotube network. The density in this diagram is normalized to the percolation threshold. The dark gray area ("subpercolation") represents films that do not have a percolative network of metallic or semiconducting tubes. The light gray area ("metallic network") represents films which are shorted out by a percolative metallic network. The green ("binary network"), light blue ("blocked semiconducting network") and dark blue ("unblocked semiconducting network") regions represent fundamentally different types of CNTN-FETs, all of which are accessible with the range of S/M ratios mentioned above. Films in the green and light blue regions feature percolative semiconducting networks blocked by Schottky barriers, while films in the dark blue region have percolative semiconducting networks that have at least some unblocked semiconducting paths through the device. The yellow dashed line and letters A−E indicates the set of points used in Figure 3. The red ellipse indicates the regime of operation for as-produced CNTN-FETs based on random networks with between roughly 67 and 89% semiconducting, (89% semiconducting reported to be the highest enriched ratio for CVD grown tubes).[27]

Downloaded by STANFORD UNIV GREEN LIBR on June 30, 2009
Published on May 13, 2009 on http://pubs.acs.org | doi: 10.1021/nl803849e

the blocked semiconducting network. The lowest proportion of semiconducting tubes that can result in any unblocked semiconducting paths is $q = 86\%$ (q_{thresh} in Figure 4). Either type of CNTN-FET, blocked or unblocked, is possible when using CNT growth processes that yield enriched semiconductor films >86% semiconducting as is possible with CVD.[27] Which type of CNTN-FET is produced will depend on the exact enrichment percentage as well as the tube density.

In conclusion, we have performed a combination of EFM and simulations that have provided new information and insights about the underlying physics of CNTN-FETs. We have shown that CNTN-FETs can exhibit sharp local voltage drops in the film, and from simulations we have determined that these drops arise from current being narrowed down to single percolative paths at certain points in the film. The associated large variations in transistor properties for the resulting devices, even for transistors with precisely identical tube length and density, has important implications for the manufacturability of such devices. For low cost solution processing methods, either larger devices will need to be made or semiconductor-enriched mixtures of tubes will need to be used, enabling higher total allowable tube densities. Finally, using a set of simple basic assumptions we have identified the different types of CNTN-FETs corresponding to different regimes of density and S/M ratio: two phases where transport through CNT film is modulated by controlling the width of Schottky barriers scattered throughout the channel and another where pure, unblocked semiconducting paths connect source to drain. The fact that these potentially very different phases of CNTN-FET operation lie relatively close together in terms of tube density and S/M ratio could help to explain the relatively large variations among reports in the literature in ON/OFF ratios and on currents for CNTN-FETs. Also, for operation in any of these phases, this work points to the advantages of purification: a higher proportion of semiconducting tubes will enable higher overall tube density without metallic shorts, resulting in higher mobilities and greater reproducibility. Further characterization of field-modulated transport between metallic and semiconducting tubes, or through semiconducting tubes crossed by metallic tubes, will lead to a fuller quantitative analysis of the pros and cons of producing CNTN-FETs in these different phases.

Acknowledgment. This work was supported by the Department of Energy, Office of Basic Energy Sciences, Division of Materials Sciences and Engineering, under contract DE-AC02-76SF00515. The improved electric force microscopy technique that enabled the potential maps was developed under support from the Center for Probing the Nanoscale, an NSF NSEC, grant PHY-0425897.

Supporting Information Available: Brief descriptions of the device fabrication, measurement of tube resistance, and the electric force microscopy technique are available. This material is available free of charge via the Internet at http://pubs.acs.org.

References

(1) Snow, E. S.; Novak, J. P.; Campbell, P. M.; Park, D. *Appl. Phys. Lett.* **2003**, *82* (13), 2145–2147.
(2) Artukovic, E.; Kaempgen, M.; Hecht, D. S.; Roth, S.; Gruner, G. *Nano Lett.* **2005**, *5* (4), 757–760.
(3) Zhou, Y.; Gaur, A.; Hur, S. H.; Kocabas, C.; Meitl, M. A.; Shim, M.; Rogers, J. A. *Nano Lett.* **2004**, *4* (10), 2031–2035.
(4) Shim, M.; Cao, M. *Adv. Mater.* **2006**, *18* (3), 304.
(5) Unalan, H. E. H. E.; Fanchini, G. G.; Kanwal, A. A.; Du Pasquier, A. A.; Chhowalla, M. M. *Nano Lett.* **2006**, *6* (4), 677–82.
(6) Kang, S. J.; Kocabas, C.; Ozel, T.; Shim, M.; Pimparkar, N.; Alam, M. A.; Rotkin, S. V.; Rogers, J. A. *Nat. Nanotechnol.* **2007**, *2* (4), 230–236.
(7) Kocabas, C. *Nano Lett.* **2007**, *7* (5), 1195.
(8) An, K. H.; Jeong, S. Y.; Hwang, H. R.; Lee, Y. H. *Adv. Mater.* **2004**, *16* (12), 1005–1009.
(9) Bekyarova, E.; Davis, M.; Burch, T.; Itkis, M. E.; Zhao, B.; Sunshine, S.; Haddon, R. C. *J. Phys. Chem. B* **2004**, *108* (51), 19717–19720.
(10) Kaempgen, M.; Roth, S. *J. Electroanal. Chem.* **2006**, *586* (1), 72–76.
(11) Hecht, D. S.; Ramirez, R. J. A.; Briman, M.; Artukovic, E.; Chichak, K. S.; Stoddart, J. F.; Gruner, G. *Nano Lett.* **2006**, *6* (9), 2031–2036.
(12) Cao, Q.; Kim, H. S.; Pimparkar, N.; Kulkarni, J. P.; Wang, C. J.; Shim, M.; Roy, K.; Alam, M. A.; Rogers, J. A. *Nature (London)* **2008**, *454* (7203), 495–U4.
(13) Zhou, X.; Park, J.-Y.; Huang, S.; Liu, J.; McEuen, P. L. *Phys. Rev. Lett.* **2005**, *95* (14), 146805.
(14) Durkop, T.; Getty, S. A.; Cobas, E.; Fuhrer, M. S. *Nano Lett.* **2004**, *4* (1), 35–39.
(15) Collins, P. G. *Science* **2000**, *287* (5459), 1801.
(16) Stadermann, M.; Papadakis, S. J.; Falvo, M. R.; Novak, J.; Snow, E.; Fu, Q.; Liu, J.; Fridman, Y.; Boland, J. J.; Superfine, R.; Washburn, S. *Phys. Rev. B* **2004**, *69*, (20), 201402.
(17) Kodama, Y.; Sato, R.; Inami, N.; Shikoh, E.; Yamamoto, Y.; Hori, H.; Kataura, H.; Fujiwara, A. *Appl. Phys. Lett.* **2007**, *91*, 133515.
(18) Kalinin, S. V.; Jesse, S.; Shin, J.; Baddorf, A. P.; Guillorn, M. A.; Geohegan, D. B. *Nanotechnology* **2004**, *15*, (8), 907−912.

(19) Appenzeller, J.; Knoch, J.; Derycke, V.; Martel, R.; Wind, S.; Avouris, P. *Phys. Rev. Lett.* **2002**, *89* (12), 126801.
(20) Fuhrer, M. S.; Nygard, J.; Shih, L.; Forero, M.; Yoon, Y. G.; Mazzoni, M. S. C.; Choi, H. J.; Ihm, J.; Louie, S. G.; Zettl, A.; McEuen, P. L. *Science* **2000**, *288* (5465), 494–497.
(21) Collins, P. C.; Arnold, M. S.; Avouris, P. *Science* **2001**, *292* (5517), 706–709.
(22) Arnold, M. S. *Nat. Nanotechnol.* **2006**, *1* (1), 60.
(23) Izard, N.; Kazaoui, S.; Hata, K.; Okazaki, T.; Saito, T.; Iijima, S.; Minami, N. *Appl. Phys. Lett.* **2008**, *92* (24), 243112.
(24) LeMieux, M. C.; Roberts, M.; Barman, S.; Jin, Y. W.; Kim, J. M.; Bao, Z. N. *Science* **2008**, *321* (5885), 101–104.
(25) Blackburn, J. L.; Barnes, T. M.; Beard, M. C.; Kim, Y. H.; Tenent, R. C.; McDonald, T. J.; To, B.; Coutts, T. J.; Heben, M. J. *ACS Nano* **2008**, *2* (6), 1266–1274.
(26) Zhang, G.; Qi, P.; Wang, X.; Lu, Y.; Li, X.; Tu, R.; Bangsaruntip, S.; Mann, D.; Zhang, L.; Dai, H. *Science* **2006**, *314* (5801), 974–977.
(27) Li, Y.; Peng, S.; Mann, D.; Cao, J.; Tu, R.; Cho, K. J.; Dai, H. *J. Phys. Chem. B* **2005**, *109* (15), 6968–6971.
(28) Li, Z. Z.; Kandel, H. R. H. R.; Dervishi, E. E.; Saini, V. V.; Xu, Y. Y.; Biris, A. R. A. R.; Lupu, D. D.; Salamo, G. J. G. J.; Biris, A. S. A. S. *Langmuir* **2008**, *24* (6), 2655–62.
(29) Bachtold, A.; Fuhrer, M. S.; Plyasunov, S.; Forero, M.; Anderson, E. H.; Zettl, A.; McEuen, P. L. *Phys. Rev. Lett.* **2000**, *84* (26), 6082.
(30) Freitag, M.; Johnson, A. T.; Kalinin, S. V.; Bonnell, D. A. *Phys. Rev. Lett.* **2002**, *89* (21), 216801.
(31) Kalinin, S. V. *Appl. Phys. Lett.* **2002**, *81* (27), 5219.
(32) Goldsmith, B.; Collins, P. Local Resistance of Single-Walled Carbon Nanotubes As Measured by Scanning Probe Techniques. In *Carbon Nanotubes*; Popov, V. N., Lambin, P., Eds.; Springer Netherlands: Dordrecht, The Netherlands, 2006; Vol. 222, pp 179−180.
(33) Staii, C.; Radosavljevic, M.; Johnson, A. Scanning Probe Microscopy of Individual Carbon Nanotube Quantum Devices. In *Scanning Probe Microscopy*; Kalinin, S., Gruverman, A., Eds.; Springer New York: New York, 2007; pp 423−439.
(34) Stadermann, M. *Phys. Rev. B: Condens. Matter* **2004**, *69* (20), 201402.
(35) Yoshihiro, K.; Ryota, S.; Nobuhito, I.; Eiji, S.; Yoshiyuki, Y.; Hidenobu, H.; Hiromichi, K.; Akihiko, F. *Appl. Phys. Lett.* **2007**, *91* (13), 133515.
(36) Hu, L.; Hecht, D. S.; Gruner, G. *Nano Lett.* **2004**, *4* (12), 2513–2517.
(37) Kumar, S.; Murthy, J. Y.; Alam, M. A. *Phys. Rev. Lett.* **2005**, *95* (6), 066802−4.
(38) Behnam, A.; Noriega, L.; Choi, Y.; Wu, Z.; Rinzler, A. G.; Ural, A. *Appl. Phys. Lett.* **2006**, *89* (9), 093107−3.
(39) Kumar, S.; Pimparkar, N.; Murthy, J. Y.; Alam, M. A. *Appl. Phys. Lett.* **2006**, *88* (12), 123505.
(40) Pimparkar, N. *IEEE Electron Device Lett.* **2007**, *28* (7), 593.
(41) Li, J.; Zhang, Z.-B.; Zhang, S.-L. *Appl. Phys. Lett.* **2007**, *91* (25), 253127.
(42) Ishida, M.; Nihey, F. *Appl. Phys. Lett.* **2008**, *92* (16), 163507.
(43) Kajiura, H.; Nandyala, A.; Coskun, U. C.; Bezryadin, A.; Shiraishi, M.; Ata, M. *Appl. Phys. Lett.* **2005**, *86* (12), 122106–3.
(44) Gao, B.; Chen, Y. F.; Fuhrer, M. S.; Glattli, D. C.; Bachtold, A. *Phys. Rev. Lett.* **2005**, *95* (19), 196802.
(45) Park, J. Y.; Rosenblatt, S.; Yaish, Y.; Sazonova, V.; Ustunel, H.; Braig, S.; Arias, T. A.; Brouwer, P. W.; McEuen, P. L. *Nano Lett.* **2004**, *4* (3), 517–520.
(46) Purewal, M. S.; Hong, B. H.; Ravi, A.; Chandra, B.; Hone, J.; Kim, P. *Phys. Rev. Lett.* **2007**, *98* (18), 186808.

NL803849E

Downloaded by STANFORD UNIV GREEN LIBR on June 30, 2009
Published on May 13, 2009 on http://pubs.acs.org | doi: 10.1021/nl803849e